

In Situ Kinetics and Mechanism of Furan Decomposition and Desorption with CO Formation on Pd(111)

Tracy E. Caldwell[†] and Donald P. Land*

Department of Chemistry, University of California, Davis, California 95616

Received: December 17, 1998; In Final Form: May 4, 1999

The work presented here uses kinetic studies under conditions of varying temperature, coverage, and isotopic substitution to elucidate the energetics and mechanism of furan decomposition and desorption on Pd(111). Laser-induced thermal desorption with Fourier transform mass spectrometry detection is used as a sensitive tool for measuring the in situ kinetics of furan decomposition simultaneously with the formation of CO. The kinetics of both furan loss and CO formation have been studied for 0.17 and 0.32 Langmuir exposures of furan on Pd(111) at 100 K. This corresponds to about 2 and 4% of a monolayer and approximately 15 and 30% of a saturation monolayer, respectively. Total observed furan loss follows two processes involving a competition between desorption and decomposition. The kinetic factors for each process are extracted yielding an activation barrier of approximately 60 kJ/mol and preexponential factor of 10^7 s^{-1} for decomposition, and an activation barrier of approximately 95 kJ/mol and preexponential factor of 10^{14} s^{-1} for desorption. The parameters for decomposition show a substantial coverage dependence at significantly less than a saturation monolayer, whereas those for desorption are relatively independent of coverage. The kinetic parameters for CO formation match those for the decomposition of furan, indicating that the rate for both reactions is limited in the same processes. Results from coverage effects and isotopic labeling experiments suggest that the rate-determining step is not simple $\alpha\text{-C-H}$ bond cleavage.

Introduction

Furan is often used in hydrodeoxygenation (HDO) studies as a model for understanding the interactions between oxygen-containing aromatic hydrocarbons and the catalytic surface of transition metals. Heteroaromatic compounds, including the sulfur- and nitrogen-containing analogues, are prevalent in crude petroleum and in liquids derived from coal and biomass.^{1,2} Their removal presents a challenge to the petrochemical industries interested in converting alternative feedstocks into useful chemicals.^{3,4} The harmful effects of these compounds (corrosion of engine parts, degradation of catalysts, and contamination of the environment) have made their removal an issue of importance. Late transition metals, such as Co or Ni, have been shown to behave as promoters in the removal process, increasing catalytic activity by about an order of magnitude.⁵ However, little is known about the surface chemistry of heterocycles on late transition metals, and even less is understood about the effects of Pd, in particular.

Previous studies by this group, using laser-induced thermal desorption (LITD), revealed interesting and unique features in the mechanism of furan decomposition on Pd(111), as illustrated in Scheme 1.^{6,7} These results have been independently confirmed in a subsequent article by Ormerod et al.⁸ The mechanism is shown to proceed at 300 K via elimination of $\alpha\text{-H}$ and CO, leaving a C_3H_3 species on the surface. Heating to 350 K causes dimerization of some of the C_3 species, forming benzene. This implies that the C_3H_3 species are stable between 300 and 350 K. Deuterium labeling studies confirm that the formation of

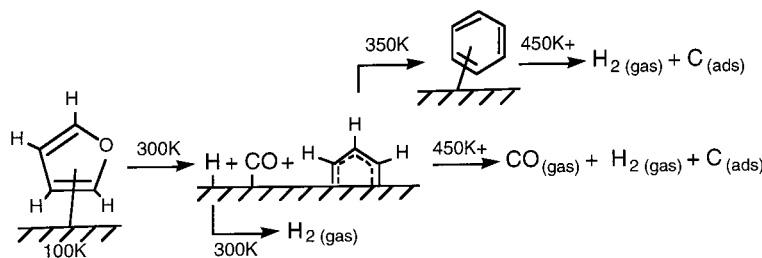
benzene proceeds via the coupling of two C_3H_3 fragments.⁶ From the standpoint of heteroatom removal, it is worth noting that oxygen is efficiently removed from the Pd(111) surface in the form of CO. In contrast to these Pd results, other late transition metals, such as clean Cu(110)⁹ and Ag(110),¹⁰ have been shown to adsorb furan reversibly with no other desorption products observed during temperature-programmed reaction (TPR). However, furan coadsorbed with oxygen on Ag(110) has been shown to produce CO_2 and H_2O , both of which are evolved starting at about 300 K during TPR.¹¹ At higher temperatures (520 K), very small amounts of partial oxidation products, such as maleic acid, benzene, and bifuran, are evolved.¹¹ The Pd surface used in our study does not require this highly oxidative environment to catalyze rapid deoxygenation of furan at 300 K. Our results also show, however, that significant amounts of carbonaceous material may be left behind on the Pd surface. These species may act to poison further catalytic reactivity unless removed, e.g., by hydrogen supplied to the feed.

For supported catalysts, Ni and Co are more effective than Zn in the promotion of the most common Mo and W HDO catalysts,¹² particularly for hydrodesulfurization (HDS) activity.^{13–16} Thus, it is reasonable to suggest that other group VII and VIII metals, such as Pd, would also serve as effective promoters for hydrotreating catalysts. Furthermore, Pd sulfides have been shown to catalyze HDS more than an order of magnitude more efficiently than sulfides of Co and Ni.¹⁷ It seems reasonable to suggest then, on the basis of the comparison of activities mentioned above, that Pd/W or Pd/Mo would have improved activities as well, perhaps surpassing the quality of the synergic contacts used most often today (i.e., Ni- and Co-promoted sulfides of W and Mo). To the best of our knowledge,

* To whom correspondence should be addressed.

[†] NASA, Johnson Space Center, Houston, TX.

SCHEME 1: Overview of Furan Decomposition Mechanism on Pd(111). Depiction of the Reaction Mechanism and Fate of Products When Furan Is Heated on Pd(111). $H_2(g)$ and $CO(g)$ Are Liberated during the Reaction, while Most of the Carbon Remains on the Surface.



though, investigations of Pd promotion of W or Mo sulfides have not yet been published.

In this paper we have pursued a more thorough understanding of the unique and unexpected reaction mechanism of furan decomposition, namely in the kinetics of the initial stage leading to CO formation. The results presented here not only help to elucidate the mechanism, but also lend valuable insight into the nature of the interactions of furan with the Pd surface. Moreover, the conclusions drawn here provide the basis for an interesting comparison between the reactivity of furan, thiophene (C₄H₄S), and pyrrole (C₄H₄NH) on Pd(111).

Experimental Section

The experiments are performed in an ultrahigh-vacuum (UHV) chamber (2×10^{-10} Torr) equipped with low-energy electron diffraction, Auger electron spectroscopy, ion sputtering, and adsorption/desorption measurements utilizing both conventional and laser-induced heating methods. Details of the apparatus were published elsewhere.^{18,19} The Pd(111) crystal surface is cleaned by repeated cycles of Ar⁺ bombardment and by heating in oxygen. Furan is purchased from Aldrich Chemical Co. (99+%) and is further purified by several freeze-pump-thaw cycles. The Pd sample is cooled to 100 K and is then dosed with furan by backfilling the chamber. Gas-phase mass spectra of furan during dosing shows that no benzene or other contaminants are present. Exposures (Langmuir = L = 10^{-6} Torr·s) have been corrected for ion gauge sensitivities. The sensitivity factor for furan (3.29) is estimated using the value listed for tetrahydrofuran, and the value for CO was assumed to be unity.²⁰

For the kinetics experiments, corrected exposures of 0.17 and 0.32 L were used. These correspond to total fluxes of (MW = 68, T(gas) = 300 K) 4.2×10^{13} and 7.9×10^{13} molecules/cm². Using a lattice parameter for Pd(111) of 2.276 Å,²¹ the surface density is 2.23×10^{15} atoms/cm². Thus, these exposures, assuming unit sticking probability, yield furan coverages of about 2 and 4% of a monolayer, respectively. On Ag(110), the saturation furan coverage corresponds to each molecule covering an area of 26 Å².¹⁰ This compares well to the area of the van der Waals perimeter for furan, which is roughly a rectangle measuring 6 by 5 Å,¹⁰ such that maximum packing would yield 3.3×10^{14} molecules/cm² or 15% of a monolayer on Pd(111). Thus, both of the coverages used here should be significantly below a saturation monolayer. Note, however, that the reliability of ionization gauges and the uncertainties involved with pressure/flux gradients in the UHV chamber could affect the accuracy of our exposure values by more than a factor of 2. Further evidence supporting our claim that these are significantly less than a saturation furan coverage comes from our thermal desorption spectroscopy (TDS) experiments. Exposures as high as 1.0 L produced no new peaks or any discernible evidence of multilayer coverage.

LITD with Fourier transform mass spectrometry (FTMS) can be used to monitor the surface composition prior to conventional desorption, and is useful in determining the mechanistic and kinetic details surrounding surface processes which are desorption-rate limited, i.e., where product evolution into the gas phase would normally follow the kinetics of desorption. LITD uses a focused, pulsed laser beam to generate a thermal spike (1000 K in 5 ns) over a 1 mm diameter spot on a surface. This phenomenal heating rate (10^{11} K/s) can access high-energy reaction pathways and typically results in desorption of species adsorbed under the laser beam before they have a chance to react.^{22–24} Many species which would react on the surface under slow heating conditions can be desorbed intact under rapid laser heating. FTMS is an ideal detection technique, because it is inherently pulsed and results in a complete (typically 10–800 Dalton), high-resolution mass spectrum^{25–28} for each single laser pulse.^{29–31}

Kinetics experiments are performed as follows. The Pd sample temperature is rapidly increased and then held constant at a temperature at which the kinetics of the reaction can be easily monitored. LITD mass spectra are obtained immediately after the desired temperature has been reached. Ideally, the sample temperature should be ramped at a sufficient rate so that the extent of reaction is small for the first laser shots. The laser is fired at a rate fast enough to accurately monitor the rapid changes in surface composition caused by reaction. Over time, the reaction slows and spectra can be taken less frequently. Many more shots are needed in the beginning to fully model the reaction rate laws and so that initial rate data can be used to determine activation energies in the event that a reaction order cannot be determined in the subsequent data analysis. The reaction is allowed to proceed for up to a full hour, and is monitored every 5–10 min to produce a clear indication that the reaction has ceased. The maximum data acquisition rate is one laser shot and mass spectrum per second. These time scales define the range of rates accessible, and therefore the temperature range.

Error bars in parameters calculated from the data are determined by Kaleidagraph (Synergy Software, Reading, PA) using a Marquardt algorithm.³² Global weighting factors are applied to transformed data (such as $w_i = y_i^2$ for logarithmic plots) and relative weighting factors ($w_i = 1/\sigma_i^2$) are applied for all data according to the uncertainties obtained in previous calculations.

Results and Discussion

CO Formation Kinetics. The time-dependent signals for both reactant (furan) and product (CO) are studied in this work. The two processes, loss of reactant and formation of product, will be addressed separately and then compared. Figure 1 shows the mass intensities for both furan and CO plotted as a function of

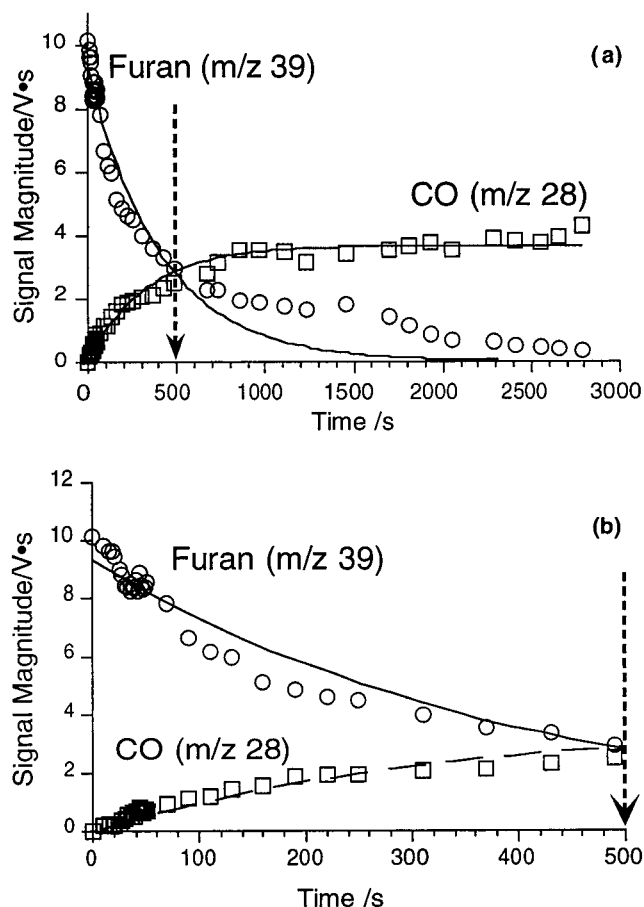


Figure 1. Furan and CO concentrations vs time at 293 K. LITD/FTMS signal magnitudes for furan (base peak is m/z 39) and CO (m/z 28) are plotted as a function of time under isothermal conditions at 293 K for a 0.17 L initial exposure of furan on Pd(111) at 100 K. This plot illustrates the simultaneous loss of furan and formation of CO. The curves are first-order exponentials, from which the data clearly deviate. Plot (b) is an expansion of the region to the left of the arrow in (a) and indicates that even the initial stages of the reaction do not follow simple first order.

time under isothermal conditions for a 0.17 L exposure of furan. Mass 39 is the largest peak in the mass spectrum for furan and is therefore followed to monitor the furan signal. However, all masses are obtained simultaneously. All masses attributed to a single component are checked to ensure that the rate of change is similar. While CO is present in the background gases of the UHV chamber, LITD with a pulsed electron beam timed to coincide with the laser pulse can discriminate between background and laser-desorbed CO. Specifically, the electron beam parameters are adjusted so that no CO is observed in the absence of a desorption laser pulse. Figure 1(a) shows clearly the decay in the furan signal simultaneously with the growth of CO. The data were initially fit assuming each process followed simple first-order kinetics. For a reaction converting species X into the species Z, the loss of reactant follows

$$[X]_t = [X]_0 e^{-kt} \quad (1)$$

and the evolution of product formation follows

$$[Z]_t = [Z]_\infty (1 - e^{-kt}) \quad (2)$$

where $[X]_t$ is the concentration of reactant at any time, t , $[X]_0$ is the initial reactant concentration, k is the first-order rate constant, $[Z]_t$ is the concentration of product at any time, t , and

$[Z]_\infty$ is the concentration of product after the reaction has gone to completion. The experimental data for the time evolution of the furan signal is fit to eq 1, using both $[X]_0$ and k as adjustable parameters, and the data for the CO signal is fit to eq 2 using both $[Z]_\infty$ and k as adjustable parameters. The curves in Figure 1 represent these first-order exponential fits. It is obvious from the plots in this figure that the simple first-order assumption is unsatisfactory. Figure 1(a) shows considerable deviation in the furan signal at later time. Figure 1(b) is an expansion of the region to the left of the arrow in Figure 1(a) with a fit to just the initial data shown, and indicates that even the early stages of the reaction do not follow the simple first-order curve. This is not too surprising if one considers that, at these temperatures, the desorption of furan is competing with the decomposition (this topic will be addressed in the following section on Furan Loss Kinetics). In addition, the buildup of products (CO, H, and presumably C_3H_3) resulting from the decomposition could significantly change the nature of the surface as a function of time.

Although the kinetics are clearly not simple first-order, the activation barrier for CO formation can be determined without any knowledge of the details of the mechanism. Assuming an arbitrary irreversible reaction,



the initial rate of reaction (κ_i) equals the initial rate of formation of Z and is simply the reaction rate constant (k) multiplied by the initial concentrations of reactants, each raised to a power appropriate for the reaction mechanism and kinetic dependence:

$$\kappa_i = k[X]_0^n \cdot [Y]_0^m \quad (4)$$

where $[X]_0$ is the initial concentration of X, and the exponents n and m may or may not be equal to the stoichiometric coefficients x and y depending on the details of the reaction mechanism. Substituting for

$$k = Ae^{-E/RT} \quad (5)$$

where A is the Arrhenius preexponential factor, E is the activation barrier for the process, R is the gas constant, and T is the absolute temperature, and taking the natural logarithm of both sides gives:

$$\ln(\kappa_i) = \{\ln(A) + \ln([X]_0^n) + \ln([Y]_0^m)\} - E/RT \quad (6)$$

The three terms in brackets on the right in eq 6 should be essentially independent of temperature for a small temperature range. One must also assume that the reaction follows van't Hoff-Arrhenius behavior and that the exponents in the rate law do not change significantly over the temperature range and coverage range used. Thus, a plot of $\ln(\kappa_i)$ vs $1/T$ should yield a straight line with a slope of $-E/R$. One can then calculate the activation energy without having to make any assumptions about the mechanism of the reaction. (However, the intercept can no longer be used to obtain the preexponential factor unless the details of the kinetic dependence and initial concentrations are known.) Figure 2 is a plot of the first 25% of the data points for a few of the isothermal kinetic experiments monitoring the formation of CO from an initial exposure of 0.17 L of furan on Pd(111). This plot illustrates that there is truly a temperature dependence on the initial rate of reaction. An Arrhenius plot of CO formation from 0.17 L exposure of C_4H_4O is shown in Figure 3. From the slope of this weighted least-squares linear regression, the activation energy was determined to be

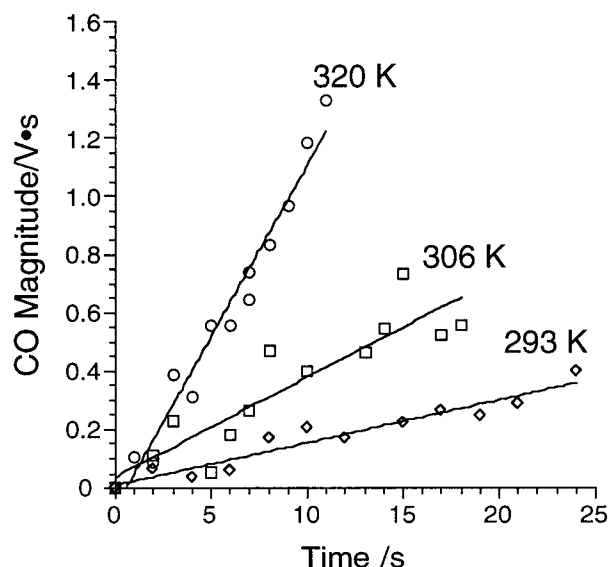


Figure 2. Initial rates of CO formation at several temperatures. Plot of the first 25% of the data points for a few of the isothermal kinetic experiments monitoring the formation of CO (m/z 28) from an initial exposure of 0.17 L furan on Pd(111) at 100 K. The data are fit to straight lines. This plot illustrates the temperature dependence of the initial rate of reaction.

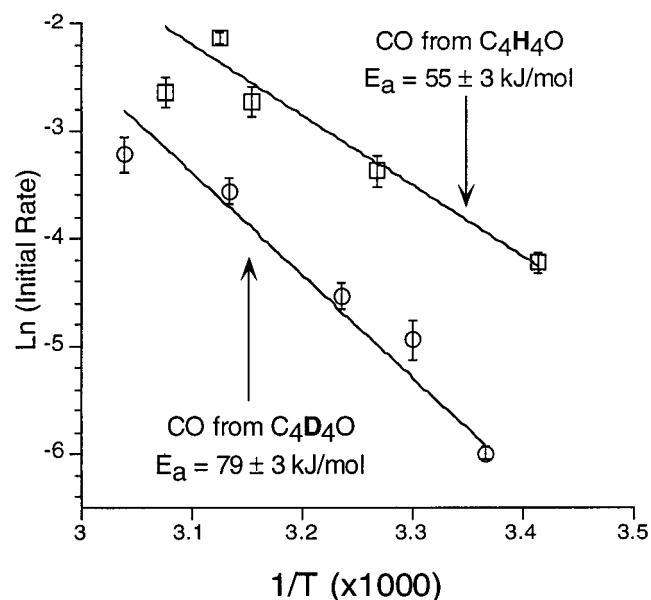


Figure 3. The Arrhenius plot gives the activation energy for CO formation from the decomposition of C_4H_4O and C_4D_4O , each obtained through separate experiments using a 0.17 L exposure of the respective furan species on Pd(111) at 100 K. From the slope of this weighted-least squares linear regression fit, an E_a of 55 ± 3 kJ/mol was obtained for the per-proteo species. An E_a of 79 ± 3 kJ/mol was obtained for the per-deutero furan.

55 ± 3 kJ/mol. Going back to the original question of how this reaction proceeds, if α -C–H bond breaking is truly the rate-determining step, then substituting each hydrogen for a deuterium should give rise to a measurable isotope effect in the kinetics.

According to transition state theory, a kinetic isotope effect (KIE) can arise from changes in vibrational zero point energies in the reactants and transition state, which is manifest in E_a shifts and differences in preexponential factors upon deuteration.^{33–35} As explained previously, no preexponential factor can be extracted from the initial rate treatment, however, any changes in E_a will give a good indication of whether a KIE exists. The

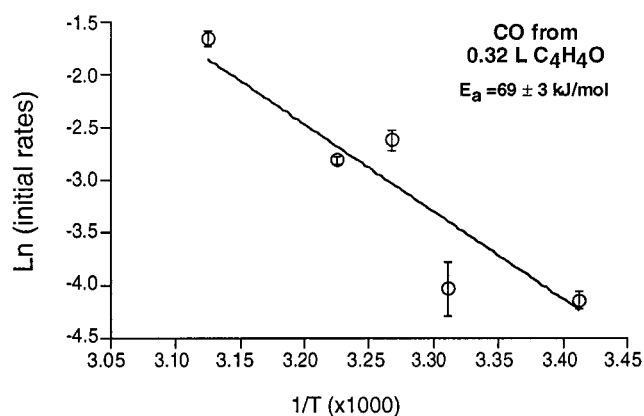


Figure 4. Coverage dependence of CO formation on initial furan exposure. The method of initial rates was used to obtain the rate data in this Arrhenius plot for 0.32 L exposure of C_4H_4O on Pd(111) at 100 K. The data are fit using a weighted least-squares linear regression to obtain $E_a = 69 \pm 3$ kJ/mol.

same kinetic experiments were run using d_4 -furan, also shown in Figure 3, and an activation energy of 79 ± 3 kJ/mol was obtained. A simple KIE could only account for a maximum of about 5 kJ/mol difference between the two activation energies (assuming that C–H(D) stretching is the reaction coordinate), and the difference observed here is about a factor of 5 greater than this. A KIE that is too large is somewhat problematic. In H/D isotope effects, tunneling is often suspected when one observes a rate for the proteo species that is significantly faster than expected. Even, for example, for $H + H_2$ vs $D + D_2$, the correction for tunneling at 300 K is a factor of 1.5 and at 200 K is only a factor of 1.7 in the rate,³⁶ whereas we see a factor in excess of 2.0 beyond the standard KIE calculated from zero point energies alone at 290 K. In addition, if tunneling were important, curvature should be observed in the Arrhenius plot.³⁷ This is not the case. These results indicate that simple C–H bond breaking is not the sole rate-determining step in the decomposition of furan to yield CO. Because all four hydrogens were replaced, a mechanism that somehow involves all or most of them could perhaps be operative. More likely, however, is that the reaction rate is not determined by a single slow step, but instead is a composite of several slow steps, each contributing to the overall rate. Isotopic substitution might then result in slowing of more than one of those steps, in addition to possibly a change in the relative contributions of the different steps. This will be discussed in more detail after the presentation of additional results.

Figure 4 is an Arrhenius plot of CO formation from C_4H_4O on Pd(111) at a higher initial exposure of furan. Initial rates were again used for these Arrhenius-type plots. Compare the E_a for the 0.17 L exposure of C_4H_4O (shown previously in Figure 3) to that obtained for a 0.32 L exposure. The activation energy for CO formation increases from 55 ± 3 to 69 ± 3 kJ/mol with only a 2-fold increase in furan exposure at low coverage. The increased barrier might arise from site blocking or a crowding-induced tilt which inhibits CO formation at higher exposures. To further elucidate this mechanism, more detailed analyses of the kinetics of furan decomposition, in conjunction with that of CO formation, are performed.

Furan Loss Kinetics. Recall from Figure 1 that the data for furan exhibited a pronounced deviation from first-order kinetics. It was discussed that the deviation might be due to a competition between furan desorption and decomposition. To account for this, a modified first-order fit was used which expresses the rate of adsorbed furan loss (observed) as the sum of two

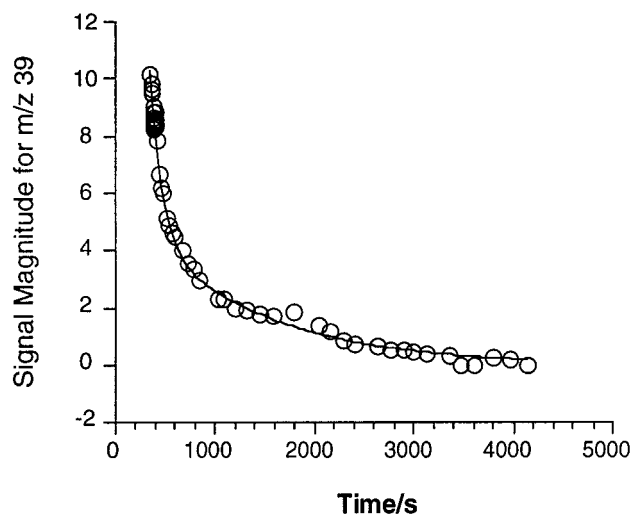


Figure 5. Loss of furan at 293 K using first-order kinetics incorporating two competing rate processes. The plot above contains the same furan loss data as that found in Figure 1 for isothermal reaction at 293 K of a 0.17 L initial exposure of furan on Pd(111) at 100 K. The data in this case are fit using a sum of two first-order kinetics processes, representing competing loss pathways, namely desorption and decomposition.

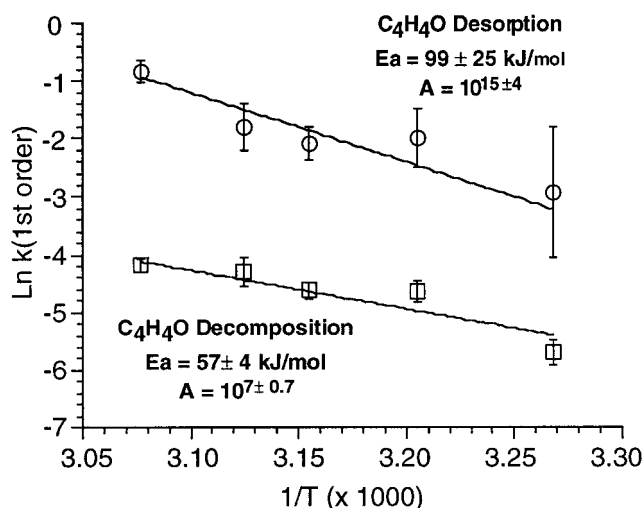


Figure 6. Arrhenius plot of furan loss kinetics using first-order kinetics with two competing rate processes. The Arrhenius plot was obtained for an initial furan exposure of 0.17 L. The two rate constants represent the desorption (circles) and decomposition (squares) pathways for furan on Pd(111).

competing rate processes:

$$-\frac{d}{dt}[\text{furan}]_{\text{ads}} = (k_{\text{des}} + k_{\text{decomp}})[\text{furan}]_{\text{ads}} = k_{\text{obs}}[\text{furan}]_{\text{ads}} \quad (7)$$

where k_{des} is the rate constant for desorption, k_{decomp} is the rate constant for decomposition, and k_{obs} is the observed rate constant for loss of adsorbed furan. With a first-order/two-parameter equation, improvement in the fit is clear, as shown in Figure 5.

Figure 6 is an Arrhenius plot of the two rate constants obtained at each temperature from this two-parameter fit using an initial furan exposure of 0.17 L on Pd(111). Notice that the plots contain information regarding the preexponential factor, A , in addition to E_a . The values calculated in this manner are reasonable. Desorption processes are typically characterized by preexponential factors in the range 10^{13} – 10^{18} s^{-1} , whereas the preexponential factor for surface reaction not involving desorption should typically have $A < 10^{11}$.

Figure 7 shows Arrhenius plots for just furan decomposition from both a 0.17 and 0.32 L exposure of $\text{C}_4\text{H}_4\text{O}$. As expected, the activation energy increases significantly with only a 2-fold increase in furan exposure and, in addition to having similar magnitudes, follows the same trend as in the CO formation rates. A slight increase in preexponential factor is also observed for furan decomposition, which may be the result of a compensation effect.^{38–40} Briefly, a decrease in activation energy can be accompanied by energetic funneling to lower states. The loss in entropy due to this funneling of energy can compensate for the decrease in E_a for that state, hence, lowering the preexponential factor as well. The coverage dependence of both routes to furan loss is summarized in Table 1.

If one compares the E_a and A for decomposition of $\text{C}_4\text{H}_4\text{O}$ and $\text{C}_4\text{D}_4\text{O}$ (separate experiments) using a 0.17 L initial exposure, again, one sees that the E_a for the proteo-species is less than that of the deuterio-species, though the magnitude for both E_a and A are much higher for the deuterio species than expected (or even what is reasonable) based on the CO data. The kinetics still do not exhibit a simple isotope effect and this inconsistency in the KIE still indicates that some factor other than simple C–H bond breaking is determining the rate of CO formation.

Also note that the values for the activation barrier obtained for the decomposition process in the loss of $\text{C}_4\text{H}_4\text{O}$ agree well with what is observed for CO formation under the same conditions of initial coverage. This is summarized in Table 2. (Recall that, because of the multiplex nature of LITD/FTMS, the signal magnitudes for both species, CO and $\text{C}_4\text{H}_4\text{O}$, were obtained simultaneously so reaction conditions are identical in both sets of data.) Because the activation energies for both $\text{C}_4\text{H}_4\text{O}$ decomposition and CO formation are identical, it is reasonable to hypothesize that both processes are moderated by the same rate-determining step. No comparison between preexponential factors can be made, however, because initial rates were used to obtain E_a for CO and preexponential factors are not obtainable.

Mechanistic Implications. Three intramolecular bonds must break to form CO, H, and C_3H_3 from furan: C–C, C–O, and C–H. It is not always the weakest bond that breaks first in a catalyzed decomposition reaction; however, if one of these bonds were significantly stronger than the other two, one would be tempted to deflect attention to the other two first. The C–C bond that must break is essentially a double bond in the free molecule (bond length of 1.361 Å).⁴¹ As such, the dissociation energy for this bond (~ 580 kJ/mol) would be much higher than that for the C–O or C–H bond (each around 400 kJ/mol). However, rehybridization upon adsorption or during reaction could make the barrier to C–C bond scission comparable to either C–O or C–H bond scission. Thus, it is not possible to categorically eliminate any of these as being the first step on the basis of bond dissociation energies. However, the measured activation energy of around 60 kJ/mol is consistent with dehydrogenation barriers, whereas it is rather low for most catalytic C–C bond breaking processes.⁴² Relatively little data exist regarding the barrier for relevant catalytic C–O bond scission, particularly because this C–O bond is part of an aromatic ring. In general, however, the reactivity of the five-membered heterocycles is dominated by reaction at the α -hydrogen, and dehydrogenation at this position is probably the initial step in the reaction.⁴³

In addition, adsorbate–Pd bonds may also need to be broken to achieve the correct orientation. Angle-resolved ultraviolet photoelectron spectroscopy (ARUPS) and high resolution

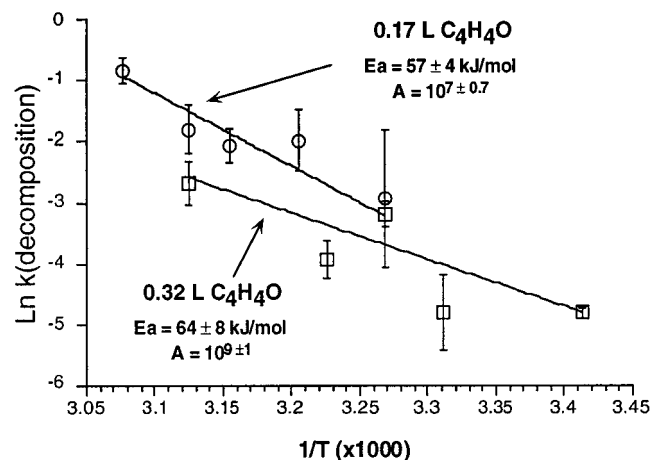


Figure 7. Coverage dependence of furan decomposition. The Arrhenius plot contains the E_a and A for furan decomposition from two different initial exposures of C_4H_4O on Pd(111) at 100 K: 0.17 L (circles) and 0.32 L (squares). The values for E_a are very close to those measured for CO formation.

TABLE 1: Coverage Dependence of Furan Desorption and Decomposition

initial furan exposure	rate constant for furan decomposition (s^{-1})	rate constant for furan desorption (s^{-1})
0.17 L	$10^{7 \pm 0.7} e^{-(57 \pm 4) \text{ kJ/mol} / RT}$	$10^{15 \pm 4} e^{-(99 \pm 25) \text{ kJ/mol} / RT}$
0.32 L	$10^{9 \pm 1} e^{-(64 \pm 8) \text{ kJ/mol} / RT}$	$10^{13 \pm 2} e^{-(92 \pm 14) \text{ kJ/mol} / RT}$

TABLE 2: Coverage Dependence of CO Formation and Furan Decomposition

initial furan exposure	CO formation E_a (kJ/mol)	furan decomposition E_a (kJ/mol)
0.17 L	55 ± 3	57 ± 4
0.32 L	69 ± 3	64 ± 8

electron energy loss spectroscopy (HREELS) studies suggest that the molecular plane of the furan molecule tilts to a significant degree on the Pd(111) surface at relatively high exposures (6–10 L).⁸ This reorientation may also contribute to the kinetics of both furan decomposition and CO formation. Consider if furan must lie flat on the surface to react. Increasing the amount of furan could hinder this process if active sites are occupied as a result (either through site blocking or lateral repulsion/attraction). Because we have measured the desorption barrier for furan to be about 90 kJ/mol, it is unlikely that the diffusion barrier is significantly greater than about 30 kJ/mol, thus it would seem that reorientation would play a minor role, at best, in the overall determination of the rate of reaction.

Comparison with Thiophene and Pyrrole Decomposition on Pd(111). The sulfur and nitrogen analogues of furan, thiophene (C_4H_4S),^{7,44,45} and pyrrole (C_4H_4NH)^{7,46} have also been studied on Pd(111), although no detailed kinetics have yet been performed. Thiophene reacts somewhat similarly to furan, decomposing at about room temperature in a ring-opening reaction. However, because of somewhat different energetics, formation of Pd–S is favored over CS, so that the products at 300 K are adsorbed S and C_4H_4 .^{7,44} Pyrrole, however, has been shown to lose the amino hydrogen at low temperatures (~200 K).^{7,46} It is thought that the remaining pyrrolyl (C_4H_4N) adsorbs with the molecular plane nearly perpendicular to the surface, because the surface–adsorbate bond here is a covalent one between N and Pd. This is in contrast to furan and thiophene, for which valence photoelectron spectroscopy shows significant bonding to the surface through the π system for both species on Pd(111), hence leading to a tilted geometry for furan⁸ and

nearly flat adsorption for thiophene.⁴⁵ This difference is evident in the very different reactivity of the C_4H_4X moiety. For furan and thiophene, ring opening and heteroatom elimination (via Pd–CO or Pd–S, respectively) occurs readily at room temperature. For pyrrole, however, these processes do not occur until about 475 K. This is consistent with decomposition of the five-membered ring requiring a nearly flat-lying geometry, a geometry much harder to achieve for the covalently bonded pyrrolyl than for furan or thiophene. The coverage-dependent studies of furan described in this article are likely to be a more subtle manifestation of a similar effect—interference with the ability of furan to lie flat.

Conclusions

The kinetics of both furan loss and CO formation have been studied for 0.17 and 0.32 L exposures of furan on Pd(111) at 100 K. This corresponds to about 2 and 4% of a monolayer and approximately 15 and 30% of a saturation monolayer, respectively. Furan loss appears to follow first-order kinetics, involving a competition between desorption and decomposition. Desorption is observed to have an activation energy of about 90 kJ/mol and a preexponential factor of $10^{14} s^{-1}$, neither of which are particularly sensitive to initial furan coverage. Furan loss via decomposition and CO product formation both have activation energies of about 55 kJ/mol at the lowest exposure and about 70 kJ/mol at twice that exposure. The similarity in activation barriers for the two processes implies that the same slow step (or steps) dictate the rate for both processes. From an initial rate treatment of isotope- and coverage-dependent data, the following have been concluded:

(a) A larger-than-expected increase in E_a upon deuteration implies that a primary KIE is not the sole factor affecting the rate, implying that α -C–H bond breaking is not the sole rate-determining step; and (b) an increase in E_a with higher exposure suggests that increasing coverage hinders the formation of CO, the barrier to which could be due to reorientation required for furan.

Acknowledgment. The authors thank the donors of the Petroleum Research Fund, administered by the American Chemical Society, and the National Science Foundation under Grant CHE-9612732 for the partial support of this research. T.E.C. also thanks the Committee on Research of UC Davis for a Graduate Research Award, and the Patricia Roberts Harris Foundation for a Graduate Fellowship Award. The authors also acknowledge I.M. Abdelrehim for his help acquiring data.

References and Notes

- (1) Furimsky, E. *Catal. Rev. Sci. Eng.* **1983**, *25*, 421.
- (2) Cadey, W. E.; Seelig, H. S. *Ind. Eng. Chem.* **1952**, *44*, 2636.
- (3) Speight, J. G. *The Desulfurization of Heavy Oils and Residua*; Marcel Dekker: New York, 1981; Vol. 4.
- (4) Kane, S. M.; Rufael, T. S.; Gland, J. L.; Huntley, D. R.; Fischer, D. A. *J. Phys. Chem. B* **1997**, *101*, 8486.
- (5) Chary, K. V. R.; Rao, K. S. R.; Muralidhar, G.; Rao, P. K. *Carbon* **1991**, *29*, 478.
- (6) Caldwell, T. E.; Abdelrehim, I. M.; Land, D. P. *J. Am. Chem. Soc.* **1996**, *118*, 907.
- (7) Caldwell, T. E.; Land, D. P. *Polyhedron* **1997**, *16*, 3197.
- (8) Ormerod, R. M.; Baddeley, C. J.; Hardacre, C.; Lambert, R. M. *Surf. Sci.* **1996**, *360*, 1.
- (9) Sexton, B. A. *Surf. Sci.* **1985**, *163*, 99.
- (10) Solomon, J. L.; Madix, R. J.; Stöhr, J. *J. Chem. Phys.* **1990**, *94*, 4012.
- (11) Crew, W. W.; Madix, R. J. *J. Am. Chem. Soc.* **1993**, *115*, 729.
- (12) Patzer, J. F.; Montagna, A. A. *Ind. Eng. Chem., Process Des. Dev.* **1980**, *19*, 382.
- (13) Furimsky, E. *AIChE J.* **1979**, *25*, 306.

- (14) Furimsky, E. *Catal. Rev.—Sci. Eng.* **1980**, 22, 371.
(15) Bussell, M. E.; Somorjai, G. A. *Catal. Lett.* **1989**, 3, 1.
(16) Ratnasany, P.; Sivasanker, S. *Catal. Rev.—Sci. Eng.* **1980**, 22, 410.
(17) Krastev, E. T.; Voice, L. D.; Tobin, R. G. *J. Appl. Phys.* **1996**, 79, 6865.
(18) Land, D. P.; Abdelrehim, I. M.; Thornburg, N. A.; Sloan, J. T. *Anal. Chim. Acta* **1995**, 307, 321.
(19) Abdelrehim, I. M.; Thornburg, N. A.; Land, D. P. *Rev. Sci. Instr.* **1997**, 68, 4572.
(20) Bartmess, J. E.; Georgiadis, R. M. *Vacuum* **1983**, 33, 149.
(21) Ohtani, H.; van Hove, M. A.; Somorjai, G. A. *Surf. Sci.* **1987**, 187, 372.
(22) Cowin, J. P.; Auerbach, D. J.; Becker, C.; Wharton, L. *Surf. Sci.* **1978**, 78, 545.
(23) George, S. M.; DeSantolo, A. M.; Hall, R. B. *Surf. Sci.* **1985**, 159, L425.
(24) Hall, R. B.; Bares, S. J. In *Chemistry and Structure at Interfaces: New Optical Probes*; Hall, R. B., Ellis, A. B., Eds.; VCH: Deerfield Beach, FL, 1986; p 85.
(25) Gross, M. L.; Rempel, D. L. *Science* **1984**, 226, 261.
(26) Wilkins, C. L.; Chowdhury, A. K.; Nuwaysir, L. M.; Coates, M. L. *Mass Spectrom. Rev.* **1989**, 8, 67.
(27) Russell, D. H. *Mass Spectrom. Rev.* **1986**, 5, 167.
(28) Marshall, A. G. *Acc. Chem. Res.* **1985**, 18, 316.
(29) Land, D. P.; Pettiette-Hall, C. L.; Hemminger, J. C.; McIver, R. T., Jr. *Acc. Chem. Res.* **1991**, 24, 42.
(30) Land, D. P.; Pettiette-Hall, C. L.; McIver, R. T., Jr.; Hemminger, J. C. *J. Am. Chem. Soc.* **1989**, 111, 5970.
(31) Land, D. P.; Pettiette-Hall, C. L.; Sander, D.; McIver, R. T., Jr.; Hemminger, J. C. *Rev. Sci. Instr.* **1990**, 61, 1674.
(32) Marquardt, D. W. *J. Soc. Ind. Appl. Math.* **1963**, II, 431.
(33) Wolfsberg, M. *Annu. Rev. Phys. Chem.* **1969**, 20, 449.
(34) Mak, C. H.; Brand, J. L.; Koehler, B. G.; George, S. M. *Surf. Sci.* **1987**, 188, 312.
(35) Madix, R. J.; Telford, S. G. *Surf. Sci.* **1992**, 277, 246.
(36) Shavitt, I. *J. Chem. Phys.* **1959**, 31, 1359.
(37) Steinfeld, J. I.; Francisco, J. S.; Hase, W. L. In *Chemical Kinetics and Dynamics*; Prentice Hall: Englewood Cliffs, NJ, 1989; p 319.
(38) Conner, W. C., Jr. *J. Catal.* **1982**, 78, 238.
(39) Fichthorn, K. A.; Weinberg, W. H. *Langmuir* **1991**, 7, 2539.
(40) Galwey, A. K. *Adv. Catal.* **1977**, 26, 247.
(41) Bak, B.; Christensen, D.; Dixon, W. B.; Henson-Nygaard, L.; Andersen, J. R.; Schottländer, M. *J. Mol. Spectrosc.* **1962**, 9, 124.
(42) Somorjai, G. A. *Introduction to Surface Chemistry and Catalysis*; Wiley: New York, 1994.
(43) Streitwieser, A., Jr.; Heathcock, C. H. In *Introduction to Organic Chemistry*, 2nd ed.; Macmillan Publishing Company: New York, 1981; p 1069.
(44) Caldwell, T. E.; Abdelrehim, I. M.; Land, D. P. *Surf. Sci.* **1996**, 367, L26.
(45) Netzer, F. P.; Bertel, E.; Goldmann, A. *Surf. Sci.* **1988**, 199, 87.
(46) Baddeley, C. J.; Hardacre, C.; Ormerod, R. M.; Lambert, R. M. *Surf. Sci.* **1996**, 369, 1.